at 3126 cm^{-1}, aromatic ring modes at 1518 cm^{-1}, and the vinyl (C=C) stretch at 1650 cm^{-1}. Unbound OTf absorptions were observed at ~1032, 1165, and 1280 cm^{-1}.
12. Elemental analysis (percent by weight) calculated for $C_{34}H_{36}Cl_8F_{12}Mo_6N_{12}O_{12}S_4$: C, 20.21; H, 1.80; N, 8.32. Found: C, 20.24; H, 1.55; N, 8.30.
13. F. A. Cotton and N. F. Curtis, *Inorg. Chem.* **4**, 241 (1965).
14. A. R. Waugh, D. R. Kingman, M. J. Hearn, D. Briggs, in *Secondary Ion Mass Spectrometry, SIMS 4*, A. Benninghoven, A. M. Huber, H. W. Werner, Eds. (Wiley, New York, 1988), pp. 231–234.
15. H. A. Hodali, H. Hung, D. F. Shriver, *Inorg. Chim. Acta* **198–200**, 245 (1992).
16. The STEM images were obtained with a Vacuum Generators HB-501A STEM equipped with an analytical pole piece (coefficient of spherical aberration C_s = 3.3 mm) at 100 keV. The theoretical resolution limit is 2.7 Å, and the pressure in a working vacuum was ~10^{-10} torr. EDAX was performed with a Link AN10000 system with a liquid nitrogen–cooled windowless Si(Li) detector. We calculated weight percent values for Mo and Cl using Cliff-Lorimer quantitative x-ray compositional analysis by Thin Film Analysis 1.3, a public domain software; *K* factors were calculated.
17. The approximate diameter of a $[Mo_6Cl_8]^{4+}$ cluster was estimated by calculation of the cubic body diagonal length (Cl–Cl = 6 Å) and the addition of two Cl^- ionic radii (Cl^- = 1.8 Å).
18. Individual clusters: theoretical percent by weight: Mo = 67, Cl = 33; EDAX percent by weight: Mo = 68 ± 8, Cl = 32 ± 2.
19. This work is dedicated to the memory of H. Deng. This work was supported by the MRL Materials Research Laboratory program of the National Science Foundation under award DMR-9121654. We thank J. Hunt, M. Thomas, and J. Silcox for aid in SEM, STEM, and EDAX analyses.

30 January 1995; accepted 10 April 1995

Ordered Metal Nanohole Arrays Made by a Two-Step Replication of Honeycomb Structures of Anodic Alumina

Hideki Masuda* and Kenji Fukuda

A highly ordered metal nanohole array (platinum and gold) was fabricated by a two-step replication of the honeycomb structure of anodic porous alumina. Preparation of the negative porous structure of porous alumina followed by the formation of the positive structure with metal resulted in a honeycomb metallic structure. The metal hole array of the film has a uniform, closely packed honeycomb structure approximately 70 nanometers in diameter and from 1 to 3 micrometers thick. Because of its textured surface, the metal hole array of gold showed a notable color change compared with bulk gold.

In recent years, there has been increasing interest in the fabrication of nanometer-sized fine structures because of their potential utilization in electronic, optical, and micromechanical devices. One approach to the fabrication of nanometer-sized structures has been to use a naturally occurring structure as a host for the fabrication (*1–6*). This approach is promising, especially for the preparation of large-area, nanometer-sized structures with high aspect ratios, which are difficult to form by a conventional lithographic process. Anodic porous alumina, which is prepared by the anodic oxidation of aluminum in an acidic electrolyte, is one of the typical self-organized fine structures with a nanohole array (*7, 8*). Anodic porous alumina has a packed array of columnar hexagonal cells with central, cylindrical, uniformly sized holes ranging from 4 to 200 nm in diameter. Many types of nanocomposites have been fabricated with anodic porous alumina used as a host material; when used for the preparation of magnetic recording media (*9, 10*), optical devices (*11*), functional electrodes (*12, 13*), and electrochromic (*14*) and electroluminescence display devices (*15*), the holes in these materials are filled with metals or semiconductors.

We have developed a process for fabricating a nanohole array in which the honeycomb structure of anodic porous alumina is replaced through a two-step molding process (*16*). In this process, fabrication of the negative type of anodic porous alumina and subsequent formation of the positive type structure led to the formation of a porous metal and semiconductor with a geometrical structure identical to that of anodic porous alumina. An important aspect that distinguishes our two-step method from the conventional one-step embedding method is that it permits the full replication of the hole array of anodic porous alumina with desired materials. In this way, it is possible to overcome the disadvantages of using porous alumina, which include insufficient chemical and thermal stability and low mechanical strength.

In our early work (*16*), the regularity of the nanohole array in the replicated structure was unsatisfactory; this resulted from imperfections in the cell arrangement in the mother anodic porous alumina used as a starting material. In recent studies, we have found that notable regularity of the cell arrangement can be accomplished under appropriate anodizing conditions. In this report, we show the fabrication of an almost ideally arranged nanohole array of metals based on the ordered porous structure of anodic alumina and describe the change in color of the metal that occurs in the nanometer-sized honeycomb structure as compared to the bulk.

An outline of the typical fabrication process is presented in Fig. 1. High-purity aluminum (99.99%) was anodized in a 0.3 M oxalic acid solution under a constant voltage of 40 V. The cell arrangement of anodic porous alumina is usually far different from the ideally packed hexagonal columnar array. We have found that anodization under appropriate conditions can produce porous alumina with a highly ordered cell configuration. This process is characterized by a longer anodization period than would normally be necessary for the preparation of porous alumina by the application of a constant appropriate anodizing voltage.

Long period anodization at 40 V improved the regularity of the cell arrangement and produced an almost ideally arranged honeycomb structure. The defect-free regions appear in large domains, whereas defects can be found at the boundaries of these domains. The size of the domains was dependent on the anodization time. That is, the size of the defect-free region increased with the anodization time. The long period anodization rearranged the cells and reduced the number of defects and dislocations. After the anodization, we obtained the starting anodic porous alumina with through holes by removing the aluminum substrate and the bottom part of the porous layer with saturated $HgCl_2$. The specimen was then dipped into a 5% (by weight) phosphoric acid solution at 30°C to adjust the pore diameter.

The two-step replication was similar to that described in (*16*). A thin metal layer (5 nm thick) was deposited on the bottom side of anodic porous alumina by vacuum deposition. Usually the same metal as that intended for use as the porous material was used for the evaporation. This thin metal layer can act as a catalyst or electrode for the subsequent metal-plating process. Methyl methacrylate monomer containing 5% (by weight) benzoyl peroxide, which acted as an initiator for polymerization, was injected into the holes under vacuum conditions and was polymerized by ultraviolet irradiation. After removal of the alumina layer with 10% (by weight) NaOH, a replicated negative type of poly(methyl methacrylate) (PMMA) with a cylindrical structure was obtained. At the bottom part of the array of PMMA cyl-

---

Department of Industrial Chemistry, Faculty of Technology, Tokyo Metropolitan University, 1-1 Minamiosawa, Hachioji, Tokyo 192-03, Japan.

*To whom correspondence should be addressed.

inders, a thin metal layer is present. For the fabrication of a Pt hole array, we used electroless deposition of Pt (*17*). After the negative type of PMMA had been dipped into the electroless plating solution, metal deposition started at the bottom part of the cylindrical structure and metal gradually filled the cavity of the PMMA to the top of the negative type of PMMA (electroless plating takes place only in the presence of a catalyst). In the preparation of a Au hole array, we adopted electrochemical metal filling and used the metal layer on the PMMA as an electrode. We could obtain the porous metal by dissolving the PMMA with acetone.

Figure 2 shows scanning electron microscopy (SEM) images of a nanohole array of Pt fabricated according to this process. We fabricated this Pt hole array using the mother porous alumina formed under the most appropriate condition at the present stage for ordering, that is, long-period anodizing for 160 hours at 0°C. From Fig. 2A, which shows the typical defect-free area of the Pt hole array, we confirm that nanoholes with uniform size are hexagonally arranged in high regularity. The regularity of the cell arrangement is exceptionally high among the naturally occurring ordered structures on the nanometer scale. The mean diameter and the interval of the holes measured from the SEM micrograph in Fig. 2A, which contains ~200 holes, were 67 ± 6 nm and 99 ± 8 nm, respectively. The mean diameter of the hole array was dependent on the condition of the dipping treatment in the phosphoric acid solution. The lower magnification image in Fig. 2B shows one of the larger domains in which the hole array is almost defect-free. This domain contains more than 1000 holes. The ordered arrangement of the hole array is maintained over the scale of several micrometers in the membrane (Fig. 2B). The cross-sectional view in Fig. 2C shows the nonintercrossing and parallel cylindrical holes that have high aspect ratios.

We have extended this process to the fabrication of a nanohole array of Au and found notable changes in the optical properties of this material, as compared with the bulk Au sample, caused by the ordered honeycomb structure. The fabricated Au specimen showed a mirror surface, because the dimensions of the geometrical structure in the hole array are sufficiently smaller than the wavelength of visible light (*18*). Figure 3 (left) shows the appearance of a Au film, the surface of which has an ordered nanohole array. Figure 3 (right) shows a sample of Au plate with a smooth surface for comparison. The Au plate with a textured hole array has a reddish color compared to the smooth Au plate.

We confirmed that the color change of Au did not originate from contamination in the electrochemically deposited Au, because the electrochemically plated Au with a smooth surface under identical plating conditions showed no distinct change of optical properties. This change in the optical properties of textured Au was analyzed by reflectance measurements in the wavelength range from 350 to 800 nm. Figure 4 shows the reflectance spectrum of the Au plate with the textured Au hole array together with that of the Au plate with the smooth surface. The spectrum of the

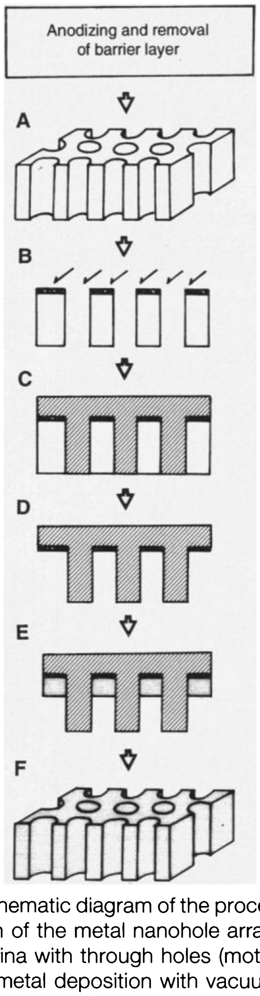

Fig. 1. Schematic diagram of the process for the fabrication of the metal nanohole array: (**A**) porous alumina with through holes (mother structure), (**B**) metal deposition with vacuum evaporation, (**C**) injection and polymerization of methyl methacrylate, (**D**) poly(methyl methacrylate) negative type, (**E**) electroless metal deposition, and (**F**) metal hole array.

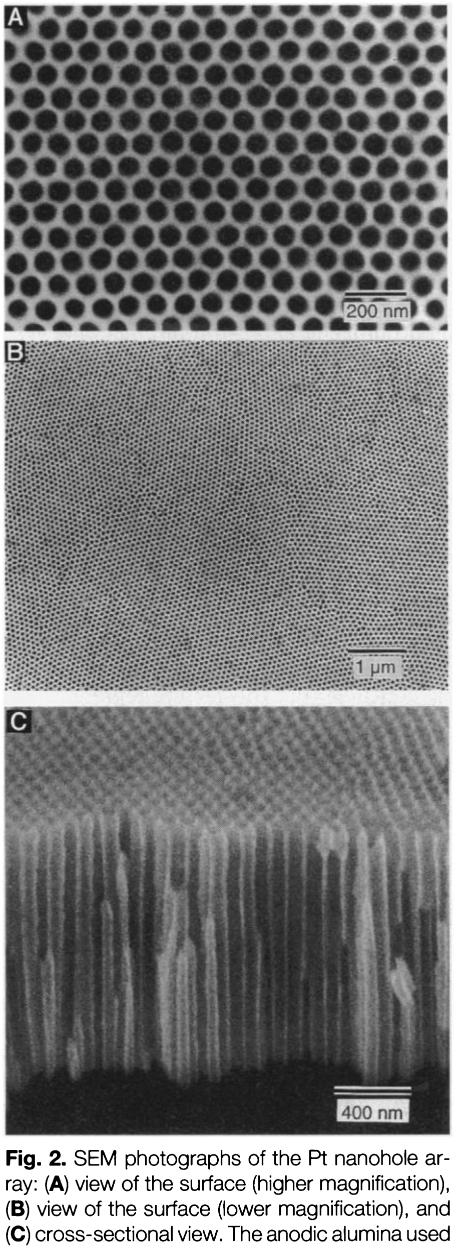

Fig. 2. SEM photographs of the Pt nanohole array: (**A**) view of the surface (higher magnification), (**B**) view of the surface (lower magnification), and (**C**) cross-sectional view. The anodic alumina used as a mother structure was formed at 0°C over a period of 160 hours. The duration of dipping treatment in phosphoric acid was 90 min.

Fig. 3. Photograph of a Au film with a textured hole array (left) and of Au plate with a smooth surface (99.9%, Nilanco, Tokyo) (right). The dimension of the hole array in the Au film is almost the same as that of Pt hole array in Fig. 2.

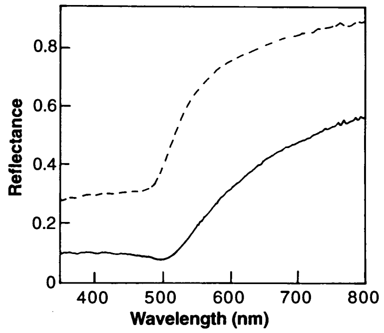

Fig. 4. Reflectance spectra of Au with a textured hole array (—) and with a smooth surface (----).

textured Au showed the relative change in the reflectance at >450 nm, which is in agreement with the observed color change in the Au plate.

Several studies have reported on the analysis of the optical properties of metal-filled anodic porous alumina; this material is typified as an array of metal particles in a dielectric medium, according to the Maxwell-Garnett and the Bruggman effective medium theory or the Mie-scattering theory (*19–21*). Our nanohole array of Au has an alternative structure: an array of air-filled holes in uniform metal. For this case the description for the inverted structure of the array of metal particles by Maxwell-Garnett theory has been reported to be applicable (*22, 23*). In the preliminary analysis of the experimental data, the qualitative shape of the reflectance spectra could be described by Maxwell-Garnett theory. For a qualitative analysis of the spectra, more detailed theories (*23, 24*) should be considered.

The process that we adopted may be useful in replacement studies of the nanostructures of other nanochannel materials (*25, 26*). Disadvantages, such as insufficient thermal and chemical stability or low mechanical strength that materials such as porous alumina might exhibit, might be overcome by this process. This nanochannel fabrication method should make it possible to fabricate nanocomposites with desired combinations of properties, a goal that has been difficult to accomplish with the conventional one-step host-guest embedding method.

REFERENCES AND NOTES

1. B. Roxlo, H. W. Deckman, J. Gland, S. D. Cameron, R. Cianelli, *Science* **235**, 1629 (1987).
2. K. Douglas, G. Devaud, N. A. Clark, *ibid.* **257**, 642 (1992).
3. G. E. Possin, *Rev. Sci. Instrum.* **41**, 772 (1970).
4. W. D. Williams and N. Giordano, *ibid.* **55**, 410 (1984).
5. C. A. Huber *et al.*, *Science* **263**, 800 (1994).
6. C.-G. Wu and T. Bein, *ibid.* **264**, 1757 (1994).
7. F. Keller, M. S. Hunter, D. L. Robinson, *J. Electrochem. Soc.* **100**, 411 (1953).
8. G. E. Thompson, R. C. Furneaux, G. C. Wood, J. A. Richardson, J. S. Gode, *Nature* **272**, 433 (1978).
9. S. Kawai and R. Ueda, *J. Electrochem. Soc.* **122**, 32 (1975).
10. M. Shiraki, Y. Wakui, T. Tokushima, N. Tsuya, *IEEE Trans. Magn.* **MAG-21**, 1465 (1985).
11. M. Saito, M. Kirihara, T. Taniguchi, M. Miyagi, *Appl. Phys. Lett.* **55**, 607 (1989).
12. C. J. Miller and M. Majda, *J. Am. Chem. Soc.* **107**, 3118 (1985).
13. M. J. Tierney and C. R. Martin, *J. Electrochem. Soc.* **137**, 3789 (1990).
14. T. Yoshino and N. Baba, *J. Chem. Soc. Jpn.* **1983**, 955 (1983).
15. I. Mizuki, Y. Yamamoto, T. Yoshino, N. Baba, *J. Metal Surf. Finish. Soc. Jpn.* **38**, 561 (1987).
16. H. Masuda, H. Tanaka, N. Baba, *Chem. Lett.* **1990**, 621 (1990); H. Masuda, K. Nishio, N. Baba, *Jpn. J. Appl. Phys.* **31**, L1775 (1992); *Thin Solid Films* **223**, 1 (1993); H. Masuda, T. Mizuno, N. Baba, T. Ohmori, *J. Electroanal. Chem.* **368**, 333 (1994).
17. The Pt was deposited at 25°C with a electroless plating solution (PT-260, NE-CHEMCAT Company, Tokyo).
18. The Au hole array was fabricated by electrochemical deposition of Au into the microcavity of the negative type of PMMA with an electroplating solution (ECF-60, NE-CHEMCAT) under the constant current condition of 4 mA cm^{-2} at 22°C. The mother anodic alumina was formed at 17°C for 7 hours, the duration of the dipping treatment in phosphoric acid being 90 min. The hole depth was 3 μm. Although the defect-free domain size of the Au hole array is smaller than that of Pt hole array and had some distortion in regularity caused by the internal stress in the electrochemically deposited Au, the pore diameter and the interval of the Au hole array were almost the same as the values for the Pt hole array shown in Fig. 2.
19. D. G. W. Goad and M. Moskovits, *J. Appl. Phys.* **49**, 2929 (1978); C. K. Preston and M. Moskovits, *J. Phys. Chem.* **92**, 2957 (1988).
20. C. G. Granqvist, A. Anderson, O. Hunderi, *Appl. Phys. Lett.* **35**, 268 (1979).
21. C. A. Foss Jr., G. L. Hornyak, J. A. Stokert, C. R. Martin, *J. Phys. Chem.* **98**, 2963 (1994).
22. G. A. Niklasson and C. G. Granqvist, *J. Appl. Phys.* **55**, 3382 (1984).
23. D. E. Aspnes, *Thin Solid Films* **89**, 249 (1982).
24. G. B. Smith, *Appl. Phys. Lett.* **35**, 668 (1979).
25. R. J. Tonucci, B. L. Justus, A. J. Campillo, C. E. Ford, *Science* **258**, 783 (1992).
26. G. Widawski, M. Rawiso, B. Francois, *Nature* **369**, 387 (1994).

5 January 1995; accepted 13 April 1995

Lehmann Discontinuity as the Base of an Anisotropic Layer Beneath Continents

James B. Gaherty* and Thomas H. Jordan

Long-period surface-wave (R_1, G_1), body-wave (*S*, *SS*, *SSS*), and *ScS*-reverberation data have been inverted to obtain anisotropic structures along seismic corridors that sample Australia and the western Pacific. These models support the proposal that the Lehmann discontinuity beneath stable continents represents a transition from an anisotropic lithosphere to a more isotropic material in the lower part of the continental tectosphere.

Lehmann (*1*) suggested that the behavior of refracted arrivals from North America and Europe at epicentral distances between 10° and 20° could be modeled by an increase in *P*-wave and *S*-wave speeds at a sharp lower boundary of the asthenospheric low-velocity zone (LVZ). Subsequent researchers argued that this Lehmann discontinuity (L) occurs globally at an average depth near 220 km (*2, 3*), and Dziewonski and Anderson (*4*) built this idea into the spherically averaged Preliminary Reference Earth Model (PREM). Solid-solid phase changes and chemical changes were ruled out as explanations (*5*), which led Hales (*3*) to conclude that this feature represents the base of a zone of partial melting, in agreement with Lehmann's basic hypothesis. However, L has not been detected in recent global stacks of long-period reflected waves (*6*), and, for a large area of the western Pacific and Australasia, it appears only on paths where the LVZ is weak or absent (*7*).

We have used new models of Australia and the western Pacific to test several alternative explanations of L that are based on the effects of seismic anisotropy. Leven *et al.* (*5*) proposed that L might be related to shear-induced anisotropy in the subcontinental mantle. From a structural model of the Australian upper mantle derived from refracted *P* waves, they hypothesized that L is the upper boundary of a thin plate-decoupling zone underlying a nearly isotropic continental mechanical boundary layer (Fig. 1A). Revenaugh and Jordan (*7*) obtained upper-mantle reflectivity profiles from vertically propagating *ScS* reverberations that indicated a ~2% increase in vertical shear (*SV*) impedance at an L with depths ranging from about 200 km along the northern Australian margin to more than 250 km beneath the Australian craton. Noting that the *SV* increase occurs near the level at which some studies of refracted *SH* waves in continents have found a shear-velocity decrease (*8*), they proposed an alternative model in which L marks the transition from an anisotropic mechanical boundary layer (MBL) to a more isotropic region below the MBL (Fig. 1B). On the basis of the apparent deepening of L toward the center of the western Australian craton, they speculated that this transition occurs at a critical temperature (near 1200°C) for the annealing of aligned textures in peridotites. They also pointed out that this horizon must be an internal feature of the continental thermal boundary layer, or tectosphere, whose thickness beneath cratons has been estimated to exceed 300 km (*9*).

Karato (*10*) accepted Revenaugh and Jordan's explanation of L as the rapid downward extinction of anisotropy, but he rejected their inference that such a feature could be maintained in a region with a low deformation rate internal to the tectosphere. Instead, he proposed that L represents the transition from dislocation-controlled creep to diffusion-controlled creep in an actively deforming asthenosphere beneath the con-

---

Department of Earth, Atmospheric, and Planetary Sciences, Massachusetts Institute of Technology, Cambridge, MA 02139, USA.

*To whom correspondence should be addressed.